Nanoporous Metal-Organic Framework Materials for Smart Applications

*Matthew R. Ryder and Jin-Chong Tan**

Department of Engineering Science, University of Oxford,
Parks Road, Oxford OX1 3PJ, United Kingdom.

corresponding author: jin-chong.tan@eng.ox.ac.uk

Abstract

This review is concerned with the recent advances in Metal-Organic Framework (MOF) materials. We highlight the unique combination of physico-chemical and thermo-mechanical characteristics associated with MOF-type materials and illustrate emergent applications in three challenging technological sectors: energy, environmental remediation and biomedicine. MOFs represent an exciting new class of nanoporous crystalline solids constituting metal ions/clusters and multifunctional organic linkages, which self-assemble at molecular level to generate a plethora of ordered 3D framework materials. The most intriguing feature of a MOF lies in its exceptionally large surface area, far surpassing those of the best activated carbon and zeolites. Next-generation multifunctional materials encompassing MOF-based thin films, coatings, membranes and nanocomposites have potential for exploitation in an immense array of unconventional applications and smart devices. We pinpoint the key technological challenges and basic scientific questions to be addressed, so as to fulfil the translational potential for bringing MOFs from the laboratory into commercial applications.

Keywords:
Metal-organic frameworks; Porous structures; Smart devices; Inorganic-organic hybrids; Multifunctionality; Porous coordination polymers.

Table of Contents

1. Introduction

The rapidly expanding field of Metal-Organic Framework (MOF) materials, or Porous Coordination Polymers (PCPs), is evidenced from the exponential growth with respect to the number of scientific publications reported and the accompanying new materials discovered over the past decade.[1] MOFs are crystalline hybrid materials constructed from inorganic and organic building blocks, *via* the fundamental process of self-assembly at the molecular level. The resulting nanoporous materials encompass a myriad of 3D open-framework structures (e.g. Fig. 1), which feature vast chemical and structural diversity.[2]

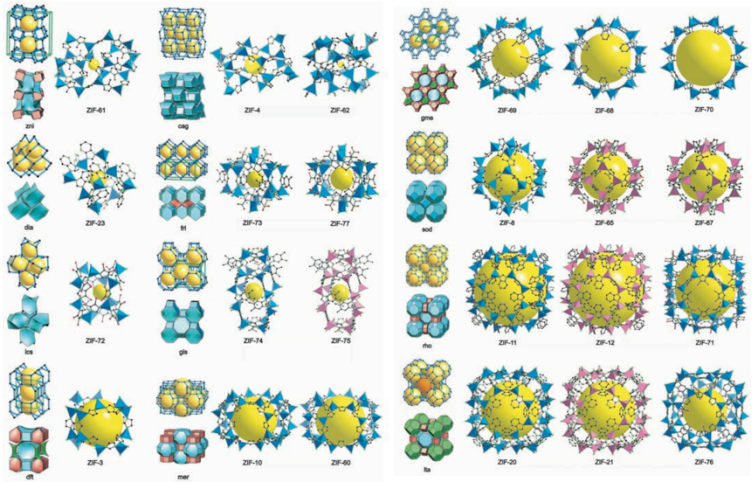

Fig. 1. Representative examples of zeolitic imidazolate framework (ZIF) materials, which are a subfamily of MOFs with diverse architectures and pore size metrics. Reprinted with permission from ref. 3.

Whilst the pioneering studies in 1990s concerned with MOFs (or PCPs[4]) were largely confined to the chemistry discipline, nowadays, research activities on MOF-type materials are extremely vibrant and highly cross-disciplinary in nature. Unquestionably the remarkably large (internal) surface areas that exist in MOFs (Fig. 2) have caught the attention and imagination of many scientists, researchers and technologists alike. Together with the capacity to precisely control and functionalise the nano-sized pore volume to yield unique multifunctional properties, the unconventional physico-chemical and thermo-mechanical characteristics of MOFs have opened up new opportunities for exploitation not only in multiple branches of chemistry, but also in the cognate fields of materials science, nanotechnology, physics, biology, medicine, and environmental engineering.

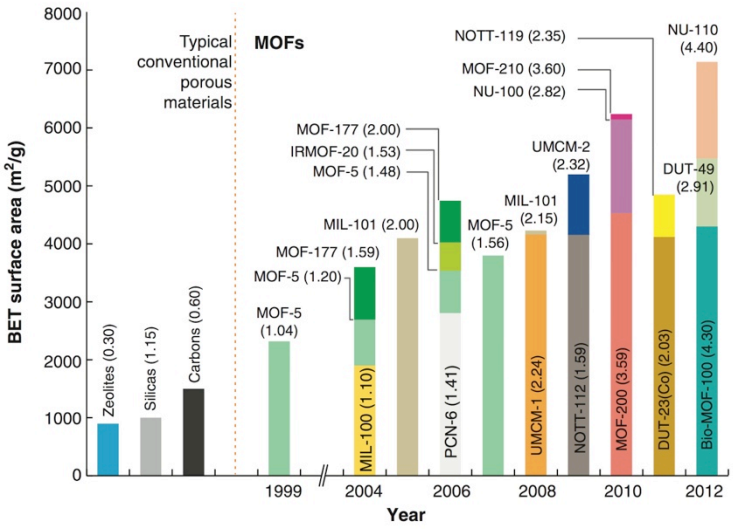

Fig. 2. Progress in the synthesis of ultrahigh-porosity MOFs. Shown here are the surface areas of MOFs in comparison with conventional porous materials (inorganic zeolites, silicas and carbons), determined from BET (Brunauer–Emmett–Teller) gas adsorption experiments. The values in parentheses indicate the pore volume in $cm^3\ g^{-1}$. Reprinted with permission from ref. 1.

From the outset, the purpose of this article is not to replicate the many excellent reviews that have already provided comprehensive coverage of specific aspects of MOF-based materials. For example, the reader may consult the following reviews which cover in detail the inorganic-organic crystal structures[5, 6] and MOF network topologies;[2] on gas adsorption characteristics,[7, 8] selective separations and gas storage capacities;[9] on luminescence[10] and chemical sensing response;[11] and also a number of critical reviews associated with thermo-mechanical behaviour,[12] ferroelectric,[13] magnetic,[14] and catalytic[15] properties of MOFs.

Our intention here is to highlight the latest exemplars associated with three prominent technological sectors — energy, environment, and biomedicine, in which multifunctional MOF-based materials may offer a new platform to enable new innovations that can be perceived as "smart applications", in the broadest sense. Furthermore, this article has been conceived such that it will be appealing to newcomers entering this exciting research field, particularly aimed at materials scientists, engineers and technologists, who have some working knowledge and interests associated with the energy, environmental, or biomedical areas.

2. Energy-Oriented Smart Applications

Research and development work focusing on renewable energy harvesting and production, storage, and conversion represents one of the global grand challenges, for which novel materials can potentially make significant contributions through the implementation of MOF-based enabling

technologies. In the sections which follow, we illustrate recent exemplars encompassing clean energy generation *via* hydrogen production, next-generation rechargeable batteries, and supercapacitors made from MOF-derived hierarchical materials.

2.1 Hydrogen Production *via* Photocatalysis

Intense research is currently being undertaken to develop innovative materials and explore green hydrogen production routes essential to afford a renewable hydrogen economy. Hydrogen is an attractive replacement for traditional fossil fuels, not only because H_2 has considerably higher energy content (e.g. nearly three times that of gasoline), but also its exhaust products comprise environmentally benign water vapour, instead of CO_2 greenhouse gas and toxic NO_x from gasoline combustion. Certain MOF-type materials[16, 17] have shown promise as photocatalyst to generate hydrogen through photochemical reduction of water under visible light irradiation. This process is also known as "water splitting", by which the water molecule is being dissociated into hydrogen and oxygen. Semiconducting titanium dioxide (TiO_2), hitherto, remains the most effective commercially available photocatalytic material.[18]

Water splitting using a photoactive MOF was first reported by Mori and co-workers in 2009,[19] who demonstrated that visible-light driven photocatalytic activity of ruthenium-based MOFs (Ru-MOF) can be highly efficient with an apparent quantum yield of 4.82% at 450 nm. While this is a relatively new direction of research, a number of excellent exemplars have emerged in the past 3-4 years,[16] where hydrogen production and photocatalytic reduction have been achieved in MOFs constituting different topologies, porosity levels, metal sites (inorganic clusters), and organic linkers, some of which coupled with postsynthetic modification (PSM).[20, 21]

Very recently, Matsuoka and co-workers[22] have studied the titanium-based MIL-125 that has been amino-functionalised, termed Ti-MOF-NH_2. Fig. 3 depicts the underlying mechanism being proposed for the hydrogen production reaction using aqueous solution containing TEOA (triethanolamine), which acts as a sacrificial electron donor under visible-light irradiation. It was proposed that the water splitting mechanism proceeds through photon absorption by the organic linker (acts as an antenna), which subsequently transfers electrons to the catalytically active inorganic Ti-oxo clusters where the protons (H^+) are finally reduced to form molecular hydrogen, H_2. Additionally, it can be seen in Fig. 4 that the photocatalytic performance of Ti-MOF-NH_2 can be substantially enhanced by depositing small quantities of platinum (up to 2 wt.% Pt) onto the parent MOF material. This study suggests that photoactive MOFs may serve as an effective nanoporous scaffold to embed co-catalysts such as Pt, by means of photodeposition.

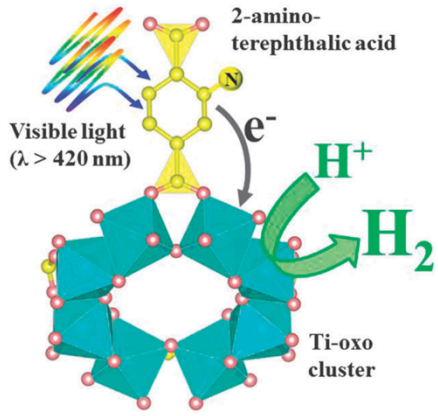

Fig. 3. Schematic illustrating the photocatalytic hydrogen production reaction in Ti-MOF-NH_2 under visible-light irradiation with a wavelength above 420 nm. Reprinted with permission from ref. [22].

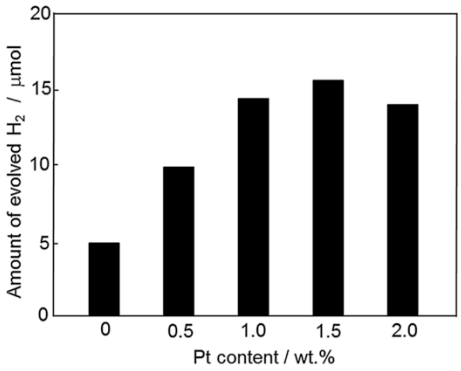

Fig. 4. Enhancing the visible-light photocatalytic hydrogen production of Ti-MOF-NH_2 by incorporating Pt (wt.%) as a co-catalyst. Reprinted with permission from ref. [22].

In a related recent study by Wang *et al.*,[23] it was shown that CdS nanoparticles (up to 50 wt.%) together with 0.5 wt.% Pt can be successfully embedded into the nanoporous structure of a Cr-based MOF (MIL-101-Cr), see Fig. 5. On its own, the as-synthesised MIL-101 material is not an effective semiconductor photocatalyst, and thus incapable of performing any water splitting (i.e. zero hydrogen evolution recorded). Notably it was found that by embedding 5 wt.% of CdS into MIL-101, the rate of H_2 generation increases from virtually zero to 22 μmol h^{-1}, while reaching the maximum capacity of ~150 μmol h^{-1} at 10 wt.% CdS. However, the water-splitting performance of the MOF photocatalyst was observed to decline at greater nanoparticles loading, which appears to resemble the findings of Matsuoka *et al.*[22] (Fig. 4); the reason behind this phenomenon remains unclear. The same enhancement strategy was further extended onto semiconducting MOF-5 and mesoporous (inorganic) zeolite MCM-41, but both systems exhibited reduced H_2 production compared with the MIL-101/CdS system.[23] Since MOF-5 is not water stable, its nanoporous framework structure is susceptible to degradation and collapse during processing and testing, thus resulting in reduced photocatalytic performance. Whilst inorganic zeolites are expected to be

thermally and chemically more superior, the reduced performance in MCM-41 was thought to be linked to its specific surface area (~940 $m^2 g^{-1}$), which is considerably lower than that of MIL-101-Cr (~4,200 $m^2 g^{-1}$). Here we note that the enormous internal surface area of a nanoporous MOF can be immediately exploited to enhance its functional performance, for which signifies a clear advantage over any other state-of-the-art photoactive materials.

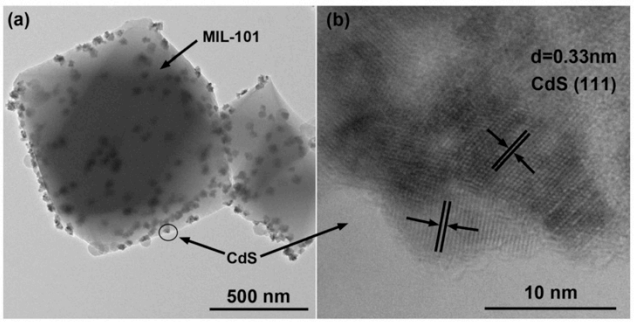

Fig. 5. (a) TEM image of CdS (10 wt.%)/MIL-101, and (b) HRTEM image of embedded CdS nanoparticles, showing their typical dimensions and morphology. Reprinted with permission from ref. [23].

Materials selection to afford water splitting practical applications obviously needs to start by screening for MOF compounds that exhibit excellent stability in aqueous solutions. To date some of the water-stable MOF materials that have been investigated for hydrogen production purposes include zeolitic imidazolate frameworks (ZIFs), particularly hydrophobic ZIF-8[24] and ZIF-9,[25] porphyrin-based MOFs,[26,27] and Zr-based MOFs especially UiO-66 and functionalised UiO-66-NH_2.[28] Outstanding materials science and practical engineering challenges include enhancing the environmental, chemical and thermo-mechanical stabilities[12] of MOF-based materials towards robust energy-harvesting apparatus, so as to warrant high efficiency and long-term durability during extended service in a large-scale industrial setting.

2.2 Electrochemical Energy Conversion and Storage

Significant advances in nanoporous MOF research have opened up a multitude of smart materials solutions to enrich the field of electrochemistry, with target applications underpinning clean energy conversion and storage. Evidently this is a rapidly expanding research topic from the fact that, in the past 3 years, at least two comprehensive review articles[16, 29] have appeared pertaining to electrochemical applications of MOFs. By virtue of this, herein we shall illustrate only the most up-to-date studies previously undescribed by the aforementioned reviews. Our discussion will encompass novel MOF-based enabling technologies and the basic science to yield clean electrochemical power sources, focusing on fuel cells, rechargeable batteries (Li-ion and Li-S) and supercapacitors.

2.2.1 Fuel cells

Whilst the fuel cell is widely recognised as an eco-friendly electrochemical conversion system, its performance is strongly dependent upon the efficiency of the electrolyte, which is a highly porous material for regulating charge transport between the anode and the cathode. By far the PEM (Proton Exchange Membrane) fuel cell has been regarded as the most promising technology for commercial implementation in the transportation sector. In order to boost the efficiency of PEM fuel cells, intense research therefore lies in the discovery and development of smart electrolyte membranes with high proton (H^+) conductivity. For a comprehensive list of proton-conducting MOFs, that have been reported up to ~2012, the reader may consult recent reviews given in refs. [16, 30]. Below we highlight a number of notable examples that have emerged only recently.

Shimizu *et al.*[31] very recently reported a new proton-conducting 3D La-based MOF, termed PCMOF-5, which features narrow 1D acidic channels housing a single column of water molecules. The material is water stable, thus it can retain structural stability in highly humid conditions omnipresent in a fuel cell environment; it is also resistant to swelling upon hydration. The proton conductivity of PCMOF-5 was determined to lie above 10^{-3} S cm^{-1} at 60 °C, under 98% relative humidity (RH). In another recent study by the same group,[32] it was demonstrated that the proton conduction of another PCMOF can be appreciably raised through an isomorphous ligand replacement strategy. The resulting mixed-ligand material, denoted as PCMOF-2½ (Fig. 6), exhibits proton conductivity of 2.1×10^{-2} S cm^{-2} (at 85 °C and 90% RH), which represents the best proton conduction value amongst proton-conducting MOFs and PCPs reported to date.[30] These materials represent examples in which the proton transport mechanism is associated with the protonic charge carriers (e.g. water, acids, and heterocycles) occupying the nanosized pores. Furthermore, by studying proton transport in a nanofilm MOF of 15-nm thickness, Kitagawa *et al.*[33] revealed that, further to the internal 1D channels, the surface of MOF nanocrystals may offer additional pathways to enhance proton conduction.

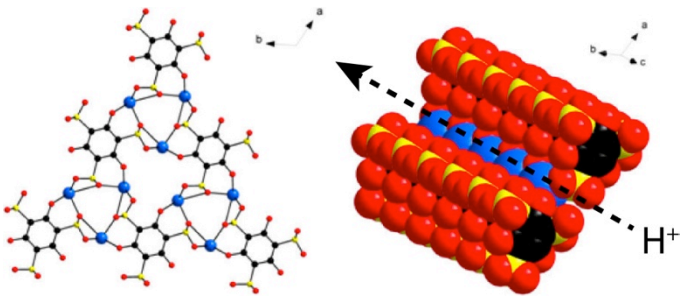

Fig. 6. Molecular structure of PCMOF-2½ showing a single pore and space-filled cross section of the 1D channel in which proton transfer takes place along the molecular chain. Adapted and reprinted with permission from ref. [32].

In another recent study, Horike *et al.*[34] demonstrated that PSM can provide a powerful approach to considerably enhance proton transport in a Ca-based MOF, featuring 1D channels. While there are guest water molecules being accommodated in the 1D channels (at 25 °C and 40% RH), the as-synthesised MOF exhibits negligibly low conductivity (5.4×10^{-9} S cm^{-1}) because these are immobilised water molecules that are strongly trapped in the pores. However, when the pores were functionalised by LiCl *via* PSM, the measured proton conductivity increased markedly to 1.8×10^{-2} S cm^{-1} at 25°C and 40% RH, and 9.0×10^{-3} S cm^{-1} at a lower 10% RH. Using pulse-field gradient NMR (Nuclear Magnetic Resonance), the authors discovered that the fast proton conductivity was achieved *via* rapid Li^+ ion mobility in the 1D channels.

2.2.2 Rechargeable batteries

The rechargeable Li-ion batteries (LIBs) are now ubiquitous in an extensive array of portable consumer electronic appliances. The standard LIB setup operates on the principle of reversible lithium (Li) insertion-extraction reaction, where the cathode material is $LiCoO_2$ while the anode is made from graphite, for which the capacities are 148 and 372 mA h g^{-1}, respectively.[29] This follows that the standard LIB capacity is, in principle, limited by the lower energy density of the cathode material. So as to enhance the capacity of LIBs, an alternative approach based on a Li alloying mechanism (or conversion reaction[35]) has shown great promise. Saravanan *et al.*[36] demonstrated successful application of Zn-formate MOF [$Zn_3(HCOO)_6$] for Li storage; notably it can be seen in Fig. 7 that beyond the first few cycles, the active material swiftly settled down to a nearly uniform capacity of 560 mA h g^{-1} for up to 60 cycles. This finding suggests that the active materials derived from Zn-formate MOFs are not only electrochemically robust, but also possess sufficient thermo-mechanical stability to retain good electrode integrity over many charge-discharge cycles.

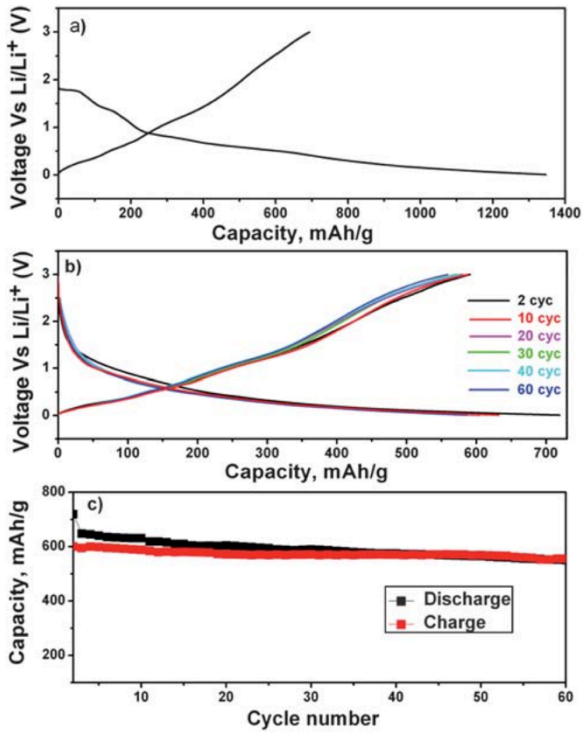

Fig. 7. Electrochemical performance of a Zn-formate MOF under a conversion reaction at constant charge-discharge current of 60 mA g^{-1}. Charge-discharge curves for the (a) first and (b) second to 60th cycles. (c) Capacity as a function of cycle number. Reprinted with permission from ref. [36].

Specifically aimed at battery-oriented applications, innovative processing routes have been developed to exploit MOFs as sacrificial templates (nanoporous precursors) to generate metal oxide nanoparticles,[37] novel nanostructures,[38-40] quantum dots,[41] high surface area nanoporous carbons,[42] and hybrid nanocomposites.[43] To illustrate this direction of work, one exciting opportunity can be seen from the very recent study by Yang *et al.*[41] where the well-known MOF-5 (or IRMOF-1) single crystals were utilised as sacrificial templates to derive hierarchically porous carbon-coated ZnO Quantum Dots (QDs) *via* pyrolysis, see Figs. 8. This low-cost and facile synthetic route yields QDs with large-surface areas associated with the small ZnO particle size of ~3.5 nm, as evidenced in Fig. 9. When tested as an LIB anode, notably such hierarchical active material exhibits high specific charge capacities (~1200 mA h g^{-1} at 75 mA g^{-1}) and good performance rate (~400 mA h g^{-1} at 3750 mA g^{-1}), in combination with good cyclability (~100% retention capacity over 50 cycles). Likewise, by employing Cu-BTC (or HKUST-1) as a sacrificial nanoporous material,[44] it has been demonstrated that this Cu-based MOF can be converted into porous CuO hollow octahedra (Fig. 10). The BET (Brunauer–Emmett–Teller) specific surface area of such novel octahedra was found to be at 49.6 m^2 g^{-1}, which is appreciably higher than any other known CuO nanostructure.[39, 40] These novel nanostructures have also been evaluated as an LIB anode material, and found to exhibit promising high-rate capacities of 351.6, 277.1 and 201.9 mA h g^{-1} corresponding to current density rates of 500, 1000, and 2000 mA g^{-1}.

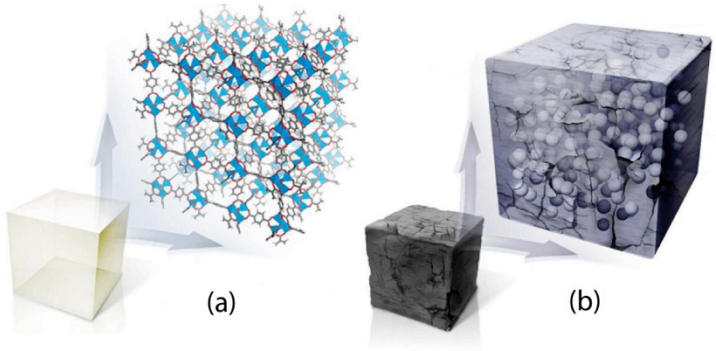

Fig. 8. Schematic illustrations of a MOF-5 single crystal (a) before and (b) after one-step controlled pyrolysis to produce carbon-coated ZnO QDs without agglomeration. The ZnO QDs are coated by a thin amorphous carbon layer that acts as a buffer layer to confine the QDs during LIB charging-discharging cycles. Reprinted with permission from ref. [41].

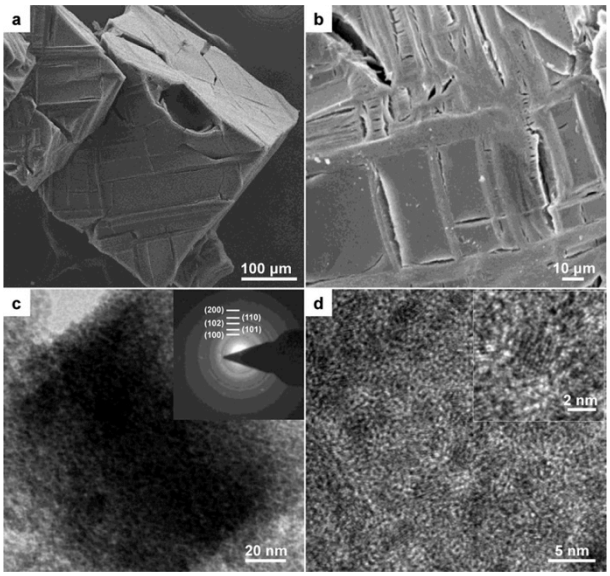

Fig. 9. ZnO QDs@porous carbon obtained by heating MOF-5 at 550 °C under an inert atmosphere: (a, b) SEM images of crystal surface morphologies; (c) TEM image (inset: SAED pattern); (d) high-resolution TEM image showing well-dispersed ZnO particles of ca. 3.5 nm (inset: enlarged view). Reprinted with permission from ref. [41].

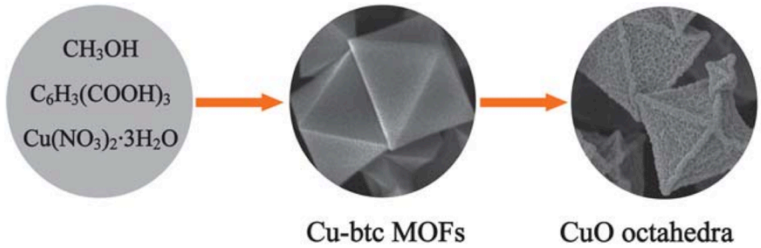

Fig. 10. Left to right: reactants for hydrothermal synthesis to generate Cu-BTC single crystals, which can then be converted into porous CuO octahedra *via* pyrolysis at 300 °C. Reprinted with permission from ref. [44].

Lithium-sulphur (Li-S) rechargeable batteries have been heralded as the next-generation electrochemical cells for high energy power systems, with great promise to succeed the conventional LIBs. Not only that Li-S cells can offer a 3~5 fold increase in energy density in comparison with LIBs,[45] the former are also considerably cheaper to manufacture due to the low cost of sulphur. However, to compensate for the poor electrical conductivity of sulphur, high surface area carbon has to be integrated into the cathodes. This aspect is precisely where hierarchically nanoporous carbon made from sacrificial MOFs can play a central role. Clearly there has been a rapid increase in research activities dealing with this materials challenge, as evidenced from the emergence of many recent reports,[46-49] which have highlighted significantly enhanced electrochemical performance of cathodes made by embedding sulphur in MOF-derived nanostructured carbonaceous materials. The performance increase can be associated with improved electron transport aided by the high surface area carbon. Furthermore, recently Xi *et al.*[48] found that the microstructures of the resulting MOF-derived carbon, i.e. both the pore volume and pore size distribution are important factors which affect the performance of the Li-S cells. In light of this, it would be advantageous to develop materials processing techniques that enable one to tune and control the precise combination of microporosity (< 2 nm) and mesoporosity (2~50 nm) that coexist in the carbonised hierarchical MOFs.

2.2.3 Supercapacitors

The supercapacitor is an electrochemical charge storage device capable of high power uptake and energy delivery, which operates either on the basis of ion adsorption in electrochemical double layer capacitors, or through fast surface redox reactions in pseudo-capacitors.[50] Recent studies have revealed that a variety of new nanoporous materials derived from MOFs are excellent platforms for application as electrodes in supercapacitors. One promising example features the conversion of cobalt-based MOFs into nanostructured Co_3O_4 (~10 nm pore size) by means of solid-state thermolysis.[51] Electrochemical tests performed on the nanoporous Co_3O_4 electrode confirmed that it can deliver a maximum specific capacitance of 150 F g^{-1} combined with excellent cyclability of over 3400 cycles at 1 A g^{-1}. A much higher specific capacitance of up to 206.76 F g^{-1} was reported for a 5-mm thickness coating comprising Co-MOF nanoparticles on an ITO (indium thin oxide) coated glass substrate.[52] Significantly, this nanostructured polycrystalline coating exhibits a good pseudo-capacitance response with excellent electrochemical redox switching, which leads to the loss of only 1.5% in capacitance upon 1000 cycles. Now we highlight an example in which high surface area nanoporous carbons were obtained through direct carbonisation of ZIF-8 (Fig. 11), which was achieved without any additional carbon sources during pyrolysis.[53] It has been found that there exists a direct correlation between the carbonisation

temperature and the resulting BET surface area of the MOF-derived carbon; when carbonised at 1000 ºC over 1000 $m^2 g^{-1}$ can be obtained. When tested as an electrode material, the electrochemical capacitance was found to be at ~200 F g^{-1}, also with good cycling stability.

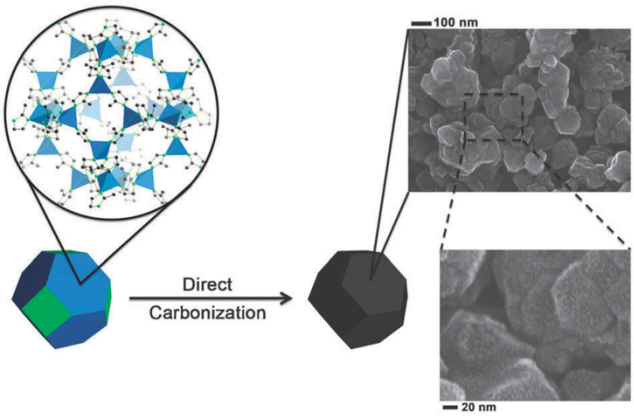

Fig. 11. Schematic illustrating preparation of nanoporous carbons through direct carbonisation of ZIF-8. SEM images corresponds to sample carbonised at 900 ºC. Reprinted with permission from ref. [53].

2.3 Microelectronics, Sensing and Transduction

Given the diverse structures and tuneable physico-chemical properties of MOFs, this new class of nanoporous materials may offer attractive new platforms to enable smart applications associated with opto-electronics, actuation and sensing technologies.

In relation to passive microelectronics, recent experimental studies[54, 55] and theoretical predictions[56] have indicated that MOFs show great potential to be exploited as low-*k* dielectrics. Electrical characterisation performed on MOF thin films have shown that the dielectric constant (*k*) of certain MOFs can potentially outperform state-of-the-art dielectrics (*k*~2.2),[57] this bodes well for future chip miniaturisation which depends on development of next-generation ultralow-*k* dielectrics. For example, Redel *et al.*[55] employed spectroscopic ellipsometry to measure the refractive index of epitaxially grown Cu-BTC (HKUST-1) thin films, from which it was estimated that the static dielectric constant is *k*~1.7. Another recent set of experiments conducted by Eslava *et al.*[54] have revealed that polycrystalline ZIF-8 thin-film coatings (see Fig. 12) exhibit excellent electrical insulating properties, for which the *k*-value was found to be 2.33 at 10^5 Hz. While these initial results appear to be promising, this topic area is at its infancy and much work remains to be done, not only in establishing underlying structure-property relationships to guide the design of improved dielectrics, but also to develop facile thin film processing techniques[58, 59] towards microelectronics fabrication.

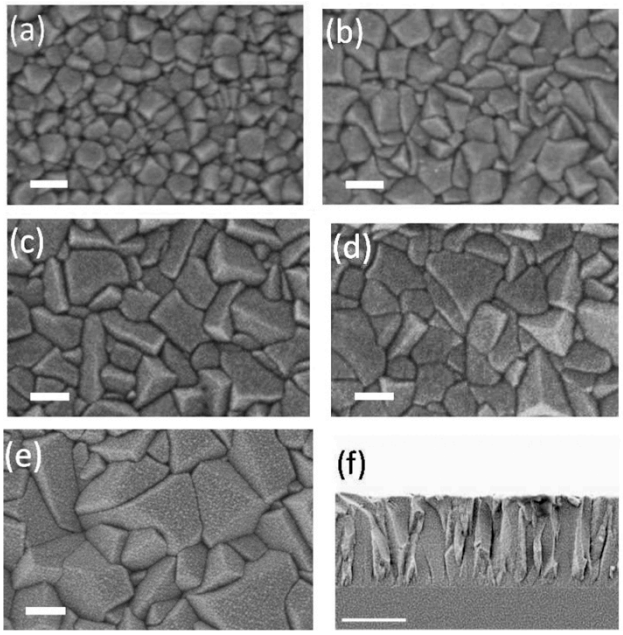

Fig. 12. SEM images of ZIF-8 films deposited on silicon wafer after different number of dip-coating cycles and the corresponding through-thickness: (a) 1 cycle, 100 nm; (b) 4 cycles, 400 nm; (c) 7 cycles, 710 nm; (d) 10 cycles, 1090 nm, and (e-g) 12 cycles, 1440 nm. Scale bar for top surface views (a-e) is 200 nm and for cross section (f) is 1000 nm. Reprinted with permission from ref. [54].

To enable the construction of active electronic devices ranging from transistors to light-emitting diodes (LEDs) and photovoltaics, a greater emphasis must be given towards the development of p-type and n-type semiconducting MOFs, the examples of which are relatively rare at present.[57, 60] More recent results include the combined experimental and theoretical studies elucidating the opportunity to tune band gaps in Zn-based MOFs,[61] where at least two strategies illustrated in Fig. 13 may be attempted during materials synthesis to: (a) control the cluster size of the secondary building units (SBU), and (b) to alternate the conjugation of the organic linkers. Since the performance of MOF active electronics will be linked to the intrinsic electrical conductivity of the nanoporous framework, an improved understanding concerned with the structure–transport property correlations and the underlying mechanisms are fundamental to realise application in microelectronics. To date only a few studies (e.g. refs. [62-64]) have explored intrinsic charge delocalisation associated with the frameworks; particularly it is not well understood whether high surface area nanoporous MOFs and hybrid materials can concurrently afford significant electrical conductivity. The latest example has been reported by Dincă *et al.*,[65] featuring a new high surface area MOF (978 $m^2 g^{-1}$) comprising 1D chains of Mn-S with high intrinsic charge mobility on par with some of the best organic semiconductors, such as polythiophenes. Another promising example features a new Fe-triazolate MOF material (termed MET-3) with permanent porosity (450 $m^2 g^{-1}$) and has a conductivity value of 0.77×10^{-4} S cm^{-1}.[66] It is not clear, however, the reason why

Fe-based MET-3 is an intrinsically conducting material whereas its Mg-, Mn-, Co-, Cu-, and Zn-counterparts lack this capability.

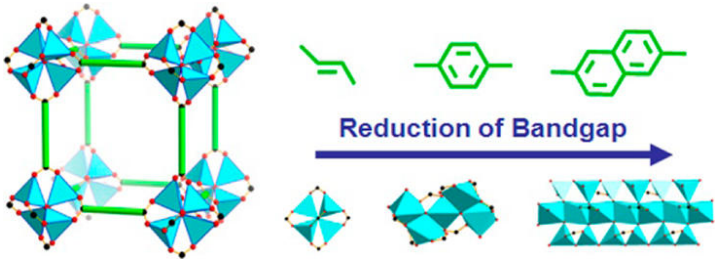

Fig. 13. Tuning the optical band gap in semiconducting Zn-MOFs, either by changing the size of the SBU clusters or by alternating the conjugation of the organic linkers (green). Reprinted with permission from ref. [61].

Smart sensors built from MOFs have attracted considerable attention in the past 5 years, leading to noteworthy proof-of-concept prototypes encompassing: (a) chemical sensors that operate on the principle of physisorption of specific guest molecules (e.g. microcantilevers in Fig. 14,[67] surface acoustic waves (SAW) sensors,[68] quartz crystal microbalances (QCM),[69] and (b) optical sensors (e.g Fabry-Pérot device[70]). For further details, it is suggested that the reader is to refer to a recent review article specific to this topic area.[11]

Because of the unique physico-chemical properties of nanoporous MOFs, there is significant potential to create miniaturised sensing devices that are extremely sensitive combined with excellent chemical selectivity and swift response time. It can be envisaged that the multifunctionality of MOFs may offer the unique opportunity to design intelligent sensors that respond to different external stimuli, for instance, optical, chemical, mechanical, thermal, electrical, or different combinations of the above. Additionally, simultaneous detection of multiple chemical species is also conceivable through an array of MEMS-based (micro-electrical-mechanical systems) microcantilever sensors, an example of which is shown in Fig. 14. The optimal design of such stress-induced chemical sensors[71] requires accurate data on mechanical properties relating to both elasticity (Fig. 15) and anelasticity of MOF-type materials, an area which is only starting to be explored either experimentally (e.g. refs. [72-74]) or computationally (e.g. refs. [75, 76]).

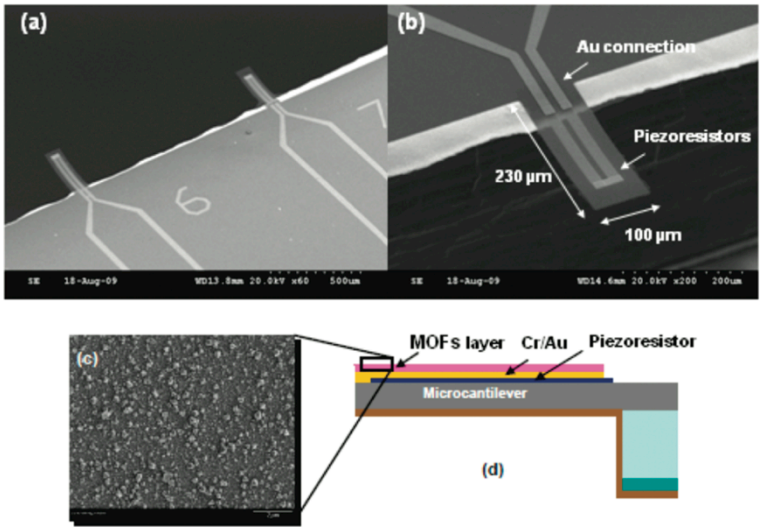

Fig. 14. (a) MEMS piezoresistive microcantilevers prior to MOF deposition. (b) The cantilever length and width were 220 µm and 100 µm, respectively. (c) SEM micrograph showing Cu-BTC thin film grown onto Au. (d) Cross-sectional diagram showing construction of the piezoresistive microcantilever. Reprinted with permission from ref. [67].

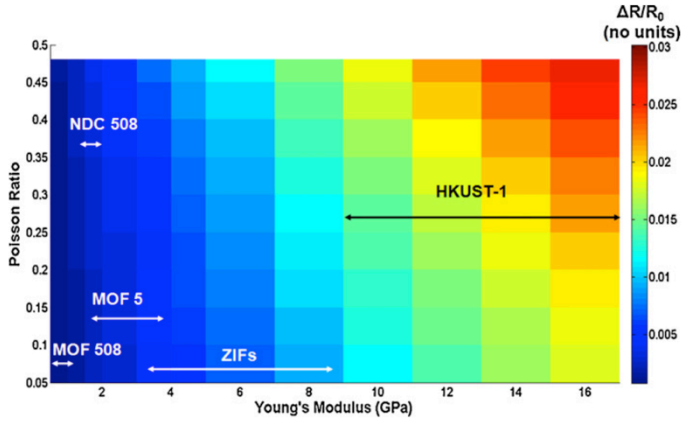

Fig. 15. MOF-based microcantilever response (finite element method predictions) as a function of different combinations of thin film elastic properties, i.e. Young's modulus or the stiffness, and the Poisson's ratio. Red indicates a stronger response, while deep blue corresponds to a weak response ($\Delta R/R_0$). Reprinted with permission from ref. [71].

3. Environmentally-Oriented Smart Applications

There is considerable interest aimed at utilising the unique properties of MOFs for a multitude of environmental applications, specifically to be used for capture and separation of various unwanted or even environmentally harmful chemicals. The advantage of MOFs over other more traditional adsorbent materials, such as zeolites and carbon black, is that they possess a far greater surface area (Fig. 2) along with well-defined pore properties.[77] It is specifically these pore properties that allow MOFs to be potentially useful for volume specific applications such as adsorption, separation and purification. The challenge is therefore to design and establish MOFs with a

specific capacity and selectivity to match the required applications, and this is now where a great deal of research is being directed.[78, 79]

3.1 Gas Adsorption, CO_2 Capture and Separation

With the demand for environmentally friendly and cost efficient applications at an all-time high, new and improved means for selective gas adsorption and separation are of great interest. In the past, adsorption based techniques have typically centred on zeolites, carbon based nanomaterials and porous silica. These have been satisfactory but there is a desire for a smarter solution that can provide better capacity and enhanced selectivity, and this is where the use of MOFs as adsorbents have shown great promise. The interactions utilised for selective gas adsorption in MOFs are primarily either by surface interactions (physisorption) or size-exclusion. The term size-exclusion, also referred to as molecular sieving, is where the substances that are excluded depend on the geometrical dimensions and morphology of the pores (e.g. aperture size and shape).

The increasing energy consumption worldwide depends primarily on combustion of fossil fuels such as coal, oil and natural gas. Unfortunately atmospheric carbon dioxide (CO_2) predominantly comes from burning these natural resources, and there is currently no economically viable alternative. Increasing levels of CO_2 in the atmosphere, intrinsically linked to climate change, has encouraged the search for improved solutions. In the past, zeolites, carbon nanotubes and silica gels have been extensively studied as adsorbents for CO_2[75, 76] however, due to low capacities and difficult regeneration processes, a smarter solution is desired. The use of MOFs has been identified as an especially promising method for the capture and sequestration (storage) of CO_2. The study of MOFs for CO_2 sequestration has become a major field of research, and readers are directed to a number of recent reviews covering more in-depth aspects (e.g. refs. [7, 80-82]), which are beyond the scope of this section.

The interest was accelerated when it was revealed that CO_2 uptakes in porous MOFs scale up with their surface areas and structures. For example, MOF-177 exhibits a Langmuir surface area of 5640 $m^2 g^{-1}$, which outperforms the other most promising, similar materials, i.e. zeolite 13X and activated carbon MAXSORB, in terms of both gravimetric and volumetric capacities, see Fig. 16.[83] At the time of writing this review, MOF-210 and MOF-200 are the currently most effective MOFs for CO_2 adsorption, both displaying a CO_2 adsorption capacity of 54.5 mmol g^{-1} (74.2 wt.%), with extremely high Langmuir surface areas of 10400 $m^2 g^{-1}$.[84] Both of which, exceed the CO_2 uptake of other previously top reported MOFs, such as MOF-177 (33.5 mmol g^{-1}, 60.8 wt.%) and MIL-101 (Cr) (40 mmol g^{-1}, 56.9 wt.%).[85, 86] NU-100 is another example of high CO_2

uptake MOF which has a CO_2 adsorption capacity of 52.6 mmol g^{-1} (69.8 wt.%) and with a BET surface area of 6143 m^2 g^{-1} (see Fig. 2).[87]

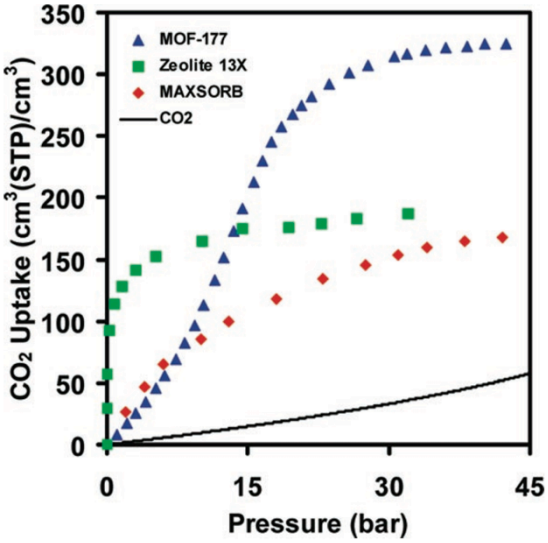

Fig. 16. Comparison of the volumetric CO_2 capacity of crystalline MOF-177 relative to zeolite 13X pellets, MAXSORB carbon powder, and pressurised CO_2. Reprinted with permission from ref. [83].

To advance the use of MOFs for CO_2 sequestration, research has been focused on a number of different approaches. This includes gaining an improved understanding of the fundamental porous framework formation and growth mechanisms, many aspects of which still remain poorly understood. Recent studies have starting to reveal that the formation mechanism of the open frameworks of MOFs may depend on multiple factors, which include metal ion coordination geometries, flexibility of the ligands, and solvent effects. The choice of solvent affecting the formation process has been shown in the past for zeolites, and more recently has also been shown to be important in the preparation of MOFs as well. By means of synchrotron-based *in situ* X-ray scattering, the complex role of solvents underpinning the nucleation and growth of two topical aluminium-based MOFs (MIL-53 and MIL-101) have recently been elucidated.[88] Another recent study involving the formation of cobalt-based MOFs,[89] through a solvothermal reaction showed that, a slight change of solvent could result in the reaction yielding multiple distinct frameworks (Fig. 17), with a range of CO_2 adsorption capabilities. This example indicates that further investigation into solvent-directed MOFs from the same reagents could be important for optimising desirable functional properties.

With the aim of enhancing the uptake of CO_2, a recent investigation into post-synthetic ceramic-like processing of MOFs, showed very promising CO_2/N_2 selectivity values, encouraging the

inclusion of such frameworks into mixed-matrix membranes in the future.[90] The second example has been concerned with the design and preparation of core-shell frameworks,[91] comprising a porous bio-MOF-11/14 mixed core with a less porous bio-MOF-14 shell, demonstrating that the shell increased CO_2 uptake by 30% compared to the core and also excluded N_2. In addition it was noted that the water-stable shell could protect the water-sensitive core. Another recent study looking to enhance selective CO_2 adsorption *via* chemical reduction of a new redox-active MOF, Zn(NDC)(DPMBI), showed that by increasing the Na^+ ion content, the CO_2 uptake in the reduced material relative to the neutral framework was enhanced up to a Na^+/Zn^{2+} molar ratio of 0.367, supporting the promise of chemical reduction of redox-active frameworks as a potential mechanism for enhancing selective CO_2 capture. Beyond this concentration, however, the surface area and CO_2 uptake decreased due to pore obstruction.[92]

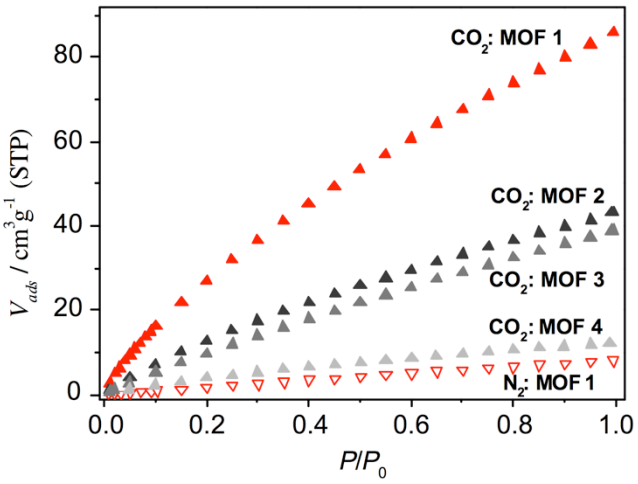

Fig. 17. CO_2 adsorption isotherms of solvent directed frameworks and N_2 adsorption isotherm of the framework with the best CO_2 adsorption capabilities. Reprinted with permission from ref. [89].

Despite their clear potential there has not been a great deal of work done on the structural stability and mechanical behaviour of MOFs at high gas pressures.[12] A recent study[93] investigating the limits and high pressure behaviour of MOF-5, showed that at high pressures of up to 225 bar, the CO_2 capacity of MOF-5 indicated fully reversible cycles without any deterioration of the uptake capacity. In addition, no credible hysteresis also indicated that a rapid pressure swing adsorption could occur. The same study did, however, identify that to avoid the structural collapse of the framework and hence maintain an efficient CO_2 capture, it was important to stay within a stability window of 3.5 hours of exposure to moist air. Lastly, they noted that the combination of techniques reported had potential to become a more generalised method for checking viability of a

sorbent for CO_2 scrubbing operations at fossil-fuel power plants, where elevated gas pressures and water-stable MOFs are essential.

Table 1. CO_2 adsorption properties for a selection of the most promising MOFs, with similar materials for comparison.

Name of compound/ MOF	Source [Ref.]	Surface area (m^2 g^{-1})		Pressure (bar)	Gravimetric CO_2 uptake (mmol g^{-1})	Temperature (K)
		BET	Langmuir			
MIL-101(Cr)	[85, 86]	4230	5900	50	40	304
MOF-177	[83]	4750	5640	42	33.5	298
NU-100	[87]	6143		40	52.6	298
MOF-210	[84]	6240	10400	50	54.5	298
MOF-200	[84]	4530	10400	50	54.5	298
Zeolite 13X	[83, 94]	616		32	7.4	
MAXSORB	[83, 95]	3300		35	25	

In the past 5 years, it is evidenced that porous MOF materials are rapidly emerging as powerful candidates for CO_2 capture and sequestration; several representative examples are given in Table 1, demonstrating that the excellent properties of MOFs have allowed them to surpass inorganic zeolites and activated carbons as the future solution to sorbent-based CO_2 capture large-scale applications.

3.2 Desalination and Water Purification

The global population is now estimated to be over 7 billion and as it continues to rise, so does the need for a solution to the issue of supplying clean water and sanitation. This section of the review will highlight the smart use of MOFs in the purification of water by identifying some recent examples in both desalination (i.e. removal of salt) and removal of toxic impurities. The supply of sufficient fresh water has long been a global issue. In the past decade, a few desalination techniques have been developed for seawater.[96] In particular, reverse osmosis currently dominates, accounting for approximately half of the installed desalination methods worldwide.[97]

MOFs may be a viable smart solution for water desalination but there has been only limited investigation into this type of application. A recent molecular simulation study investigating the capability of a ZIF-8 membrane for desalination supports the claim.[98] The work indicated that desalination can occur under external pressure, involving Na^+ and Cl^- ions being unable to pass through the membrane due to a molecular sieving effect. ZIF-8 was chosen due to its chemical and thermal stability[99, 100] providing it remarkably resistant to water and organic solvents, largely due

to the hydrophobic pores. However, it is worth pointing out that, the presence of certain limitations in the study including the use of a rigid framework and the assumption that the membrane material is entirely defect free (i.e. presence of cracks will permit ions to pass unimpeded). The absence of framework flexibility could portray an unrealistic rate of molecular salt sieving, and this is where additional theoretical work has been concentrated.[101]

Lately there has also been research into the removal of dye materials,[102] considered to be toxic and even carcinogenic, from aqueous solution. The potential of MIL-101 has been identified for the removal of both methyl orange (MO)[103] and xylenol orange,[104] due to its excellent adsorption properties. More recently, the use of MOF-235 has also shown promise for the removal of MO, as well as methylene blue,[105] through electrostatic interactions between the dyes and the adsorbent. In another recent example, MIL-100(Fe) has been suggested for the removal of malachite green.[106]

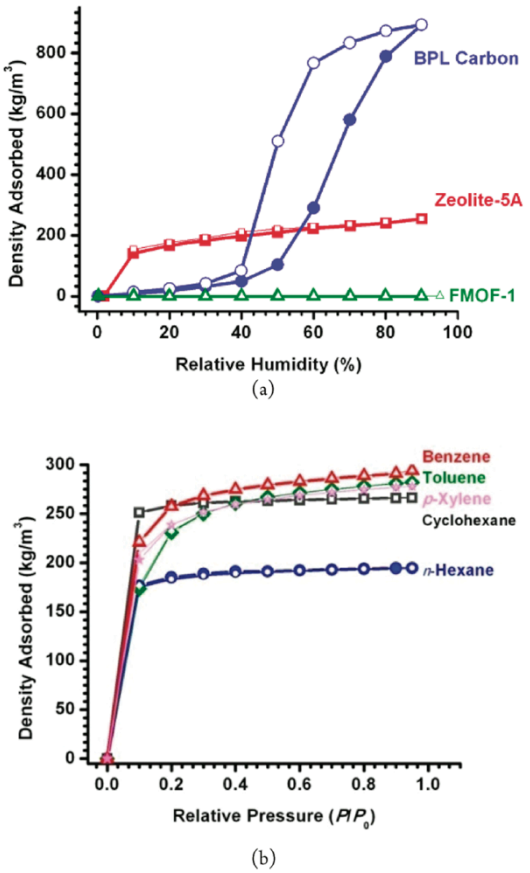

Fig. 18. (a) Water adsorption isotherms for FMOF-1, zeolite-5A, and BPL carbon. (b) Oil components adsorption in FMOF-1 using vapours of cyclohexane, n-hexane, benzene, toluene, and p-xylene. Open symbols indicate desorption. Reprinted with permission from ref. [107].

The liquid-phase adsorptive removal of naproxen and clofibric acid, two typical PPCPs (pharmaceuticals and personal care products), has recently been studied using MOFs, namely,

MIL-101-Cr and MIL-100-Fe.[108] It was suggested that MOFs possessing high porosity along with large pore size can be potential adsorbents to remove harmful PPCPs from contaminated water.

Research has suggested that MOFs with a high capacity and affinity to C_6-C_8 hydrocarbons could be the future of oil spill recovery. It has been demonstrated that FMOF-1, a fluorous MOF, exhibits reversible adsorption with a high capacity for n-hexane, cyclohexane, benzene, toluene, and p-xylene, with no detectable water adsorption even at near 100% relative humidity. This significantly outperforms other porous materials such as, activated carbon and zeolites, as shown in Fig. 18. In addition, FMOF-2, obtained from the annealing of FMOF-1, was shown to have enlarged cages and channels with double the amount of toluene adsorption, when compared with FMOF-1.[107] Removal of other hazardous materials such as sulphur containing compounds,[109, 110] heavy metal ions,[111] bisphenol-A,[112] volatile iodine,[113, 114] and microcystin[115] have also recently been studied.

4. Biomedical-Oriented Smart Applications

Recently MOFs have been suggested for a range of biomedical applications, such as delivery of therapeutic agents, due in part to their high capacity and tuneability. MOFs exhibit many desired characteristics as drug carriers, including exceptionally high surface areas and large pore sizes for drug encapsulation, intrinsic biodegradability and versatile (multi)functionality. A large number of guests can be entrapped within the MOFs, including conventional drugs and gasotransmitter gases. The biological application of MOFs is still quite new, but research so far has produced promising results.

4.1 Drug Encapsulation Properties

Latest studies has focused on expanding the current understanding of encapsulation properties in terms of both uptake and release of novel compounds within MOFs. It has been shown recently that the most relevant chemical and structural features of a series of functionalised MOFs can significantly impact their performance as candidates for delivery of compounds including caffeine and ibuprofen.[116, 117] It was shown that tuning the polarity, polarisability, and hydrogen donor ability of terephtalate linkers present in the flexible MIL-88-Fe framework, has enabled for optimisation of caffeine uptake, as shown in Fig. 19.[116] However this response was not applicable to all framework topologies, as demonstrated for the UiO-66 framework where the same chemical

features were no longer the driving force, concluding that rationalisation of the encapsulation properties was more complex.

Work continued into the confinement of caffeine in UiO-66 frameworks, with different functional groups.[118] It was shown that caffeine molecules preferentially located in the smaller cages, giving rise to only weak interactions with the functional groups grafted onto the organic linker. Dielectric relaxation measurements further revealed significant modifications of the ligand dynamics during the drug encapsulation for all UiO-66-Zr structures. It was evident that the functional group, whatever its polarity, did not serve as a significantly attractive site for the drug, although the caffeine primarily adsorbs in the vicinity of the organic linker.

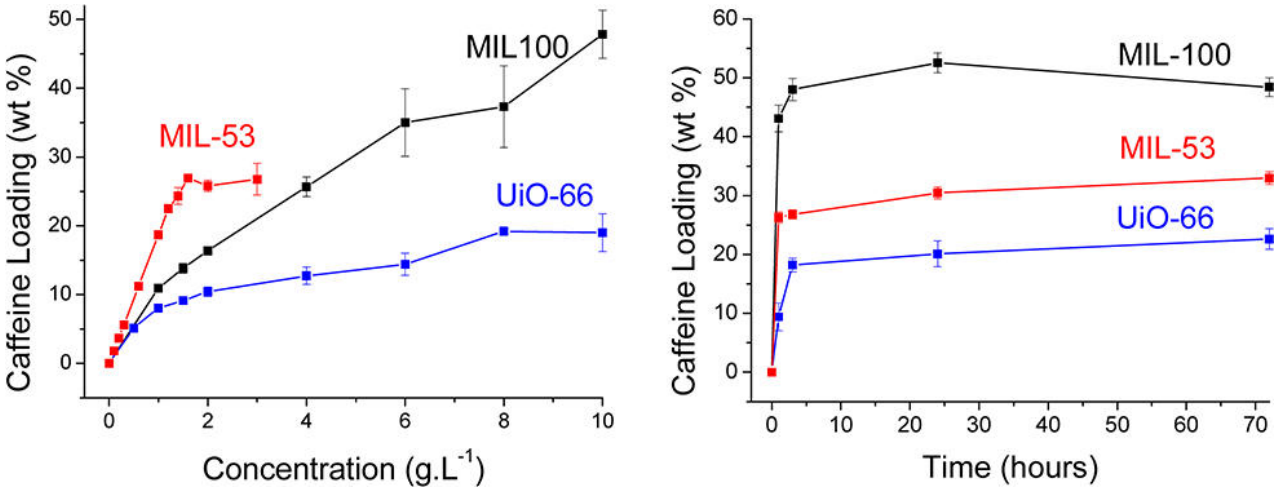

Fig. 19. Room-temperature caffeine adsorption isotherms (left) and kinetics of encapsulation (right) for MIL-100, UiO-66, and MIL-53. Reprinted with permission from ref. [119].

Another recent study investigating the driving force of encapsulation and the kinetics of delivery showed caffeine successfully entrapped within frameworks, achieving exceptional payloads of up to 50 wt.%, together bearing very fast kinetics of encapsulation.[119] The work showed the release of caffeine strongly depended on the specific release media (MOF stability, caffeine mobility, and MOF-caffeine interactions). With the ability to control the release within 8-24 hours, MIL-100 and UiO-66 appear to be promising carriers for the administration of caffeine with both spectacular payloads and progressive releases.

4.2 Encapsulation and Delivery

A molecular docking method was recently used for the identification of drug molecules (ibuprofen, methylene blue, amoxicillin, and gentamicin) with high affinities for the [Zn(BDC)(H_2O)$_2$]n framework.[120] The work involved estimating the binding affinity differences

for the individual classes of guest molecules and the approach proved to provide a fast and affordable alternative to current experiments for identification of the binding preferences of a host system for a set of guest molecules, with the possibility of decreasing the timeframe of certain screening processes.

It has been demonstrated recently that the protein cytochrome c (Cyt c) can enter the interior of a MOF despite the significantly large protein dimensions.[121] It was suggested that Cyt c must undergo significant conformational distortion to allow for entry through the relatively small microporous windows. The results of fluorescence studies further suggested that Cyt c undergoes conformational changes during the immobilisation process and adopts a unique conformation unseen before. The use of MOF materials for protein translocation requires further investigation but the preliminary results are encouraging. Another study demonstrated organic acids such as acetic and benzoic acid could be utilised to form zinc based MOFs of theophylline.[122] The work showed theophylline could be released rapidly in simulated gastroenteric fluid and a slowed release of theophylline could be obtained from all frameworks in pure water; suggesting a new strategy for the release of drug molecules in a controlled manner.

4.3 Storage and Delivery of Gasotransmitter Gases

Given that large surface area MOFs can possess excellent gas storage properties, it is reasonable to extend the functionality into biological applications, such as gaseous therapeutics. It has been shown that MOFs can perform exceptionally well for nitric oxide (NO),[123] far outperforming previous materials, such as inorganic zeolites.[124] It was demonstrated that stored gas could be available for delivery even after the material has been stored for several months, with a simple gas recovery, triggered by water.[125] The combination of extremely high adsorption capacity and good storage stability is ideal for a NO storage material, as shown in Fig. 20.

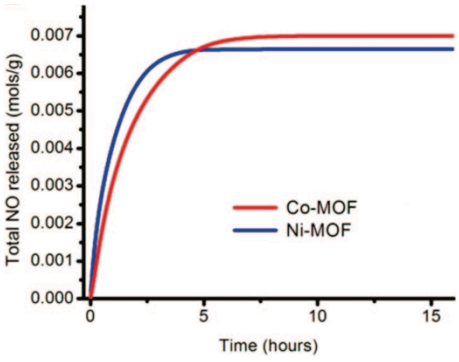

Fig. 20. The total amounts of NO released by two MOFs, normalised per gram of activated solid. Reprinted with permission from ref. [125].

Carbon monoxide (CO) binding has been shown to occur to unsaturated coordination sites of MOFs.[126] The release of CO from MIL-88B-Fe and NH2-MIL-88B-Fe was found to be controlled by the degradation of the frameworks under physiological conditions. Controlled CO-release was shown by modifying the frameworks, by the introduction of additional amino groups. Given that both structures have good biocompatibility, it would suggest that MOFs could serve as good CO-delivery systems in therapeutic applications. MOFs with the CPO-27 structure have also been shown to bind with hydrogen sulphite, allowing for storage of at least several months.[127]

4.4 Biosensing and Toxicity

MOFs have been reported as promising delivery devices in medical imaging,[128, 129] including computed tomography,[130] where iodinated MOFs were shown to completely degrade within 46 hours; a desirable property for medicinal imaging agents.[131] Recent work has involved the use of MOFs specifically for the bio-sensing of HIV DNA, based on recognition of duplex DNA (ds-DNA). The study showed that in the presence of the target ds-DNA, a TFO (triplex-forming oligonucleotide) probe could interact with ds-DNA to form a rigid triplex structure, resulting in fluorescence recovery.[132] The detection limit of HIV DNA from this approach is promising and would suggest additional follow-up studies.

In vivo toxicity of high doses of nanoparticles from three different iron based MOFs (MIL-88A, MIL-88B-4CH_3 and MIL-100) was recently investigated by evaluating their distribution, metabolism and excretion.[133] All studied parameters (serum, enzymatic, histological) indicated low acute toxicity. The MOFs were degraded into their constitutive components, allowing for the removal of the carboxylic linkers along with excess iron, by excretion. The work confirmed the interest of the use of biodegradable non-toxic iron(III) carboxylate MOF nanoparticles for biomedical applications.

The ability to enclose both therapeutic drugs and imaging agents has identified MOFs as a promising candidate for a multitude of smart biological applications. However, applications of the bulk MOFs (i.e. powdered form) are limited for real life medicinal application. The bulk MOFs need to be scaled down (e.g. nanoparticles) so that the resulting NanoMOFs[134] can circulate systemically while maintaining the advantageous properties of the bulk. A lot of the work remaining to be done involves scaling down to NanoMOFs and further understanding and predicting the stability of the materials and their potential toxicity. The preliminary results on both

fronts are positive, as mentioned above, but with all medicinal research the requirements to move the work from fundamental studies to clinical trials are high.

5. Concluding Remarks and Outlook

This review has covered the potential applications of MOFs within the energy industry, through research reported in areas such as renewable hydrogen production, next-generation rechargeable batteries, and novel supercapacitors. It has identified benefits within the environmental remediation and sustainability sectors, through work involved in CO_2 sequestration and water purification. It has also explained how MOFs can benefit biological sciences, specifically medicine, through work involved in drug delivery and biosensing. The diverse range of smart applications and technological innovations discussed throughout this review exemplify the substantial contribution MOF materials may offer to a multitude of different scientific disciplines, including but not limited to, chemistry, materials science, engineering, nanotechnology, physics, biomedicine, and environmental science. The vast and cross-disciplinary research evidenced thus far supports the claim that: MOFs are a promising next-generation material with amazing versatility and capacity to tackle a number of global challenges of the 21st century.

The amount of high-quality research being done on MOFs has witnessed exceptional growth in the past 15 years, and it is foreseeable that this upward trend will continue accelerating into the next decade. Although we expect work to continue to be focused on the discovery of new materials and related fundamental studies, the trend is certainly shifting towards utilising the materials for the many potential applications it can be applied to. The pioneers and research community involved with MOFs have made tremendous progress in establishing a very promising field, which is now at a crossroad where it can make a significant impact within the technology sector. It is exhilarating to anticipate what smart applications and new innovations will be discovered next, and to see MOFs being used in the applications we highlighted on a commercial scale.

References

1. H. Furukawa, K. E. Cordova, M. O'Keeffe, and O. M. Yaghi, *Science*, 2013, **341**, 974-986.
2. A. K. Cheetham, C. N. Rao, and R. K. Feller, *Chem. Commun.*, 2006, 4780-4795.
3. R. Banerjee, A. Phan, B. Wang, C. Knobler, H. Furukawa, M. O'Keeffe, and O. M. Yaghi, *Science*, 2008, **319**, 939-943.
4. B. F. Hoskins and R. Robson, *J. Am. Chem. Soc.*, 1990, **112**, 1546-1554.
5. D. J. Tranchemontagne, J. L. Mendoza-Cortes, M. O'Keeffe, and O. M. Yaghi, *Chem. Soc. Rev.*, 2009, **38**, 1257-1283.
6. M. O'Keeffe and O. M. Yaghi, *Chem. Rev.*, 2012, **112**, 675-702.
7. K. Sumida, D. L. Rogow, J. A. Mason, T. M. McDonald, E. D. Bloch, Z. R. Herm, T. H. Bae, and J. R. Long, *Chem. Rev.*, 2012, **112**, 724-781.
8. M. P. Suh, H. J. Park, T. K. Prasad, and D.-W. Lim, *Chem. Rev.*, 2012, **112**, 782-835.
9. J.R. Li, J. Sculley, and H.-C. Zhou, *Chem. Rev.*, 2012, **112**, 869-932.
10. Y. Cui, Y. Yue, G. Qian, and B. Chen, *Chem. Rev.*, 2012, **112**, 1126-1162.
11. L. E. Kreno, K. Leong, O. K. Farha, M. Allendorf, R. P. Van Duyne, and J. T. Hupp, *Chem. Rev.*, 2012, **112**, 1105-1125.
12. J. C. Tan and A. K. Cheetham, *Chem. Soc. Rev.*, 2011, **40**, 1059-1080.
13. W. Zhang and R.-G. Xiong, *Chem. Rev.*, 2012, **112**, 1163-1195.
14. M. Kurmoo, *Chem. Soc. Rev.*, 2009, **38**, 1353-1379.
15. J. Lee, O. K. Farha, J. Roberts, K. A. Scheidt, S. T. Nguyen, and J. T. Hupp, *Chem. Soc. Rev.*, 2009, **38**, 1450-1459.
16. S.L. Li and Q. Xu, *Energy Environ. Sci.*, 2013, **6**, 1656-1683.
17. J.L. Wang, C. Wang, and W. Lin, *ACS Catalysis*, 2012, **2**, 2630-2640.
18. Y. Horiuchi, T. Toyao, M. Takeuchi, M. Matsuoka, and M. Anpo, *Phys. Chem. Chem. Phys.*, 2013, **15**, 13243-13253.
19. Y. Kataoka, K. Sato, Y. Miyazaki, K. Masuda, H. Tanaka, S. Naito, and W. Mori, *Energy Environ. Sci.*, 2009, **2**, 397-400.
20. A. P. Smalley, D. G. Reid, J.-C. Tan, and G. O. Lloyd, *CrystEngComm*, 2013.
21. M. Nasalevich, M. Goesten, T. J. Savenije, F. Kapteijn, and J. Gascon, *Chem. Commun.*, 2013.
22. T. Toyao, M. Saito, Y. Horiuchi, K. Mochizuki, M. Iwata, H. Higashimura, and M. Matsuoka, *Catal. Sci. Technol.*, 2013, **3**, 2092-2097.
23. J. He, Z. Yan, J. Wang, J. Xie, L. Jiang, Y. Shi, F. Yuan, F. Yu, and Y. Sun, *Chem. Commun.*, 2013, **49**, 6761-6763.
24. D. Esken, H. Noei, Y. M. Wang, C. Wiktor, S. Turner, G. Van Tendeloo, and R. A. Fischer, *J. Mater. Chem.*, 2011, **21**, 5907-5915.
25. Q. Li and H. Kim, *Fuel Process. Technol.*, 2012, **100**, 43-48.
26. A. Fateeva, P. A. Chater, C. P. Ireland, A. A. Tahir, Y. Z. Khimyak, P. V. Wiper, J. R. Darwent, and M. J. Rosseinsky, *Angew Chem Int Ed Engl*, 2012, **51**, 7440-7444.
27. Y. Liu, Y. Yang, Q. Sun, Z. Wang, B. Huang, Y. Dai, X. Qin, and X. Zhang, *ACS Appl. Mater. Interfaces*, 2013, **5**, 7654-7658.
28. C. G. Silva, I. Luz, F. X. Llabres i Xamena, A. Corma, and H. Garcia, *Chem. Eur. J.*, 2010, **16**, 11133-11138.
29. A. Morozan and F. Jaouen, *Energy Environ. Sci.*, 2012, **5**, 9269-9290.
30. M. Yoon, K. Suh, S. Natarajan, and K. Kim, *Angew. Chem. Int. Ed.*, 2013, **52**, 2688-2700.
31. J. M. Taylor, K. W. Dawson, and G. K. H. Shimizu, *J. Am. Chem. Soc.*, 2013, **135**, 1193-1196.
32. S. Kim, K. W. Dawson, B. S. Gelfand, J. M. Taylor, and G. K. H. Shimizu, *J. Am. Chem. Soc.*, 2013, **135**, 963-966.
33. G. Xu, K. Otsubo, T. Yamada, S. Sakaida, and H. Kitagawa, *J. Am. Chem. Soc.*, 2013, **135**, 7438-7441.
34. S. Horike, Y. Kamitsubo, M. Inukai, T. Fukushima, D. Umeyama, T. Itakura, and S. Kitagawa, *J. Am. Chem. Soc.*, 2013, **135**, 4612-4615.
35. J. Cabana, L. Monconduit, D. Larcher, and M. R. Palacin, *Adv. Mater.*, 2010, **22**, E170-192.
36. K. Saravanan, M. Nagarathinam, P. Balaya, and J. J. Vittal, *J. Mater. Chem.*, 2010, **20**, 8329-8335.
37. X. Xu, R. Cao, S. Jeong, and J. Cho, *Nano Letters*, 2012, **12**, 4988-4991.
38. L. Zhang, H. B. Wu, S. Madhavi, H. H. Hng, and X. W. Lou, *J. Am. Chem. Soc.*, 2012, **134**, 17388-17391.
39. L. Hu, Y. Huang, F. Zhang, and Q. Chen, *Nanoscale*, 2013, **5**, 4186-4190.
40. Z. Yuan, Y. Wang, and Y. Qian, *RSC Advances*, 2012, **2**, 8602.
41. S. J. Yang, S. Nam, T. Kim, J. H. Im, H. Jung, J. H. Kang, S. Wi, B. Park, and C. R. Park, *J. Am. Chem. Soc.*, 2013, **135**, 7394-7397.
42. W. Chaikittisilp, K. Ariga, and Y. Yamauchi, *J. Mater. Chem. A*, 2013, **1**, 14-19.
43. X. Zheng, Y. Li, Y. Xu, Z. Hong, and M. Wei, *Crystengcomm*, 2012, **14**, 2112-2116.
44. R. Wu, X. Qian, F. Yu, H. Liu, K. Zhou, J. Wei, and Y. Huang, *J. Mater. Chem. A*, 2013, **1**, 11126-11129.

45. X. L. Ji, S. Evers, R. Black, and L. F. Nazar, *Nat. Commun.*, 2011, **2**, 1-7.
46. G. Xu, B. Ding, L. Shen, P. Nie, J. Han, and X. Zhang, *J. Mater. Chem. A*, 2013, **1**, 4490-4496.
47. W. Xia, B. Qiu, D. Xia, and R. Zou, *Sci. Rep.*, 2013, **3**, 1-7.
48. K. Xi, S. Cao, X. Peng, C. Ducati, R. V. Kumar, and A. K. Cheetham, *Chem. Commun.*, 2013, **49**, 2192-2194.
49. H. B. Wu, S. Wei, L. Zhang, R. Xu, H. H. Hng, and X. W. Lou, *Chem. Eur. J.*, 2013, **19**, 10804-10808.
50. P. Simon and Y. Gogotsi, *Nat. Mater.*, 2008, **7**, 845-854.
51. F. Meng, Z. Fang, Z. Li, W. Xu, M. Wang, Y. Liu, J. Zhang, W. Wang, D. Zhao, and X. Guo, *J. Mater. Chem. A*, 2013, **1**, 7235-7241.
52. D. Y. Lee, S. J. Yoon, N. K. Shrestha, S. H. Lee, H. Ahn, and S. H. Han, *Microporous Mesoporous Mat.*, 2012, **153**, 163-165.
53. W. Chaikittisilp, M. Hu, H. Wang, H. S. Huang, T. Fujita, K. C. Wu, L. C. Chen, Y. Yamauchi, and K. Ariga, *Chem. Commun.*, 2012, **48**, 7259-7261.
54. S. Eslava, L. Zhang, S. Esconjauregui, J. Yang, K. Vanstreels, M. R. Baklanov, and E. Saiz, *Chem. Mater.*, 2013, **25**, 27-33.
55. E. Redel, Z. Wang, S. Walheim, J. Liu, H. Gliemann, and C. Woell, *Appl. Phys. Lett.*, 2013, **103**.
56. K. Zagorodniy, G. Seifert, and H. Hermann, *Appl. Phys. Lett.*, 2010, **97**, 251905.
57. M. D. Allendorf, A. Schwartzberg, V. Stavila, and A. A. Talin, *Chemistry*, 2011, **17**, 11372-11388.
58. D. Witters, S. Vermeir, R. Puers, B. F. Sels, D. E. De Vos, J. Lammertyn, and R. Ameloot, *Chem. Mater.*, 2013, **25**, 1021-1023.
59. C. Hou, Q. Xu, J. Peng, Z. Ji, and X. Hu, *ChemPhysChem*, 2013, **14**, 140-144.
60. C. Gomes Silva, A. Corma, and H. Garcia, *J. Mater. Chem.*, 2010, **20**, 3141-3156.
61. C.-K. Lin, D. Zhao, W.-Y. Gao, Z. Yang, J. Ye, T. Xu, Q. Ge, S. Ma, and D.-J. Liu, *Inorg. Chem.*, 2012, **51**, 9039-9044.
62. Y. Kobayashi, B. Jacobs, M. D. Allendorf, and J. R. Long, *Chem. Mater.*, 2010, **22**, 4120-4122.
63. M. Hmadeh, Z. Lu, Z. Liu, F. Gandara, H. Furukawa, S. Wan, V. Augustyn, R. Chang, L. Liao, F. Zhou, E. Perre, V. Ozolins, K. Suenaga, X. Duan, B. Dunn, Y. Yamamto, O. Terasaki, and O. M. Yaghi, *Chem. Mater.*, 2012, **24**, 3511-3513.
64. T. C. Narayan, T. Miyakai, S. Seki, and M. Dinca, *J. Am. Chem. Soc.*, 2012.
65. L. Sun, T. Miyakai, S. Seki, and M. Dinca, *J. Am. Chem. Soc.*, 2013, **135**, 8185-8188.
66. F. Gandara, F. J. Uribe-Romo, D. K. Britt, H. Furukawa, L. Lei, R. Cheng, X. Duan, M. O'Keeffe, and O. M. Yaghi, *Chem. Eur. J.*, 2012, **18**, 10595-10601.
67. J. H. Lee, R. T. J. Houk, A. Robinson, J. A. Greathouse, S. M. Thornberg, M. D. Allendorf, and P. J. Hesketh, *Micro- and Nanotechnology Sensors, Systems, and Applications*, 2010, **7679**.
68. A. L. Robinson, V. Stavila, T. R. Zeitler, M. I. White, S. M. Thornberg, J. A. Greathouse, and M. D. Allendorf, *Anal. Chem.*, 2012, **84**, 7043-7051.
69. R. Ameloot, L. Stappers, J. Fransaer, L. Alaerts, B. F. Sels, and D. E. De Vos, *Chem. Mater.*, 2009, **21**, 2580-2582.
70. G. Lu and J. T. Hupp, *J. Am. Chem. Soc.*, 2010, **132**, 7832-7833.
71. A. Venkatasubramanian, J.-H. Lee, V. Stavila, A. Robinson, M. D. Allendorf, and P. J. Hesketh, *Sens. Actuator B-Chem.*, 2012, **168**, 256-262.
72. B. Van de Voorde, R. Ameloot, I. Stassen, M. Everaert, D. De Vos, and J.-C. Tan, *J. Mater. Chem. B*, 2013, **1**, 7716-7724.
73. J. C. Tan, B. Civalleri, C. C. Lin, L. Valenzano, R. Galvelis, P. F. Chen, T. D. Bennett, C. Mellot-Draznieks, C. M. Zicovich-Wilson, and A. K. Cheetham, *Phys. Rev. Lett.*, 2012, **108**.
74. J. C. Tan, P. Jain, and A. K. Cheetham, *Dalton Trans.*, 2012, **41**, 3949-3952.
75. H. Wu, T. Yildirim, and W. Zhou, *J. Phys. Chem. Lett.*, 2013, **4**, 925-930.
76. V. Ishwar Hegde, J.-C. Tan, U. V. Waghmare, and A. K. Cheetham, *The Journal of Physical Chemistry Letters*, 2013, 130923010300004.
77. G. Férey, *Chem. Soc. Rev.*, 2008, **37**, 191-214.
78. R. L. Martin and M. Haranczyk, *J. Chem. Theory Comput.*, 2013, **9**, 2816-2825.
79. L. C. Lin, A. H. Berger, R. L. Martin, J. Kim, J. A. Swisher, K. Jariwala, C. H. Rycroft, A. S. Bhown, M. W. Deem, M. Haranczyk, and B. Smit, *Nat. Mater.*, 2012, **11**, 633-641.
80. D. M. D'Alessandro, B. Smit, and J. R. Long, *Angew Chem Int Ed Engl*, 2010, **49**, 6058-6082.
81. Y. S. Bae and R. Q. Snurr, *Angew Chem Int Ed Engl*, 2011, **50**, 11586-11596.
82. J. Liu, P. K. Thallapally, B. P. McGrail, D. R. Brown, and J. Liu, *Chem. Soc. Rev.*, 2012, **41**, 2308-2322.
83. A. R. Millward and O. M. Yaghi, *J. Am. Chem. Soc.*, 2005, **127**, 17998-17999.
84. H. Furukawa, N. Ko, Y. B. Go, N. Aratani, S. B. Choi, E. Choi, A. O. Yazaydin, R. Q. Snurr, M. O'Keeffe, J. Kim, and O. M. Yaghi, *Science*, 2010, **329**, 424-428.
85. P. L. Llewellyn, S. Bourrelly, C. Serre, A. Vimont, M. Daturi, L. Hamon, G. De Weireld, J. S. Chang, D. Y. Hong, Y. Kyu Hwang, S. Hwa Jhung, and G. Ferey, *Langmuir*, 2008, **24**, 7245-7250.
86. G. Férey, C. Mellot-Draznieks, C. Serre, F. Millange, J. Dutour, S. Surble, and I. Margiolaki, *Science*, 2005, **309**, 2040-2042.

87. O. K. Farha, A. O. Yazaydin, I. Eryazici, C. D. Malliakas, B. G. Hauser, M. G. Kanatzidis, S. T. Nguyen, R. Q. Snurr, and J. T. Hupp, *Nat. Chem.*, 2010, **2**, 944-948.
88. M. G. Goesten, E. Stavitski, J. Juan-Alcañiz, A. Martiñez-Joaristi, A. V. Petukhov, F. Kapteijn, and J. Gascon, *Catal. Today*, 2013, **205**, 120-127.
89. P.-Z. Li, X.-J. Wang, Y. Li, Q. Zhang, R. H. D. Tan, W. Q. Lim, R. Ganguly, and Y. Zhao, *Microporous Mesoporous Mat.*, 2013, **176**, 194-198.
90. W. M. Bloch, R. Babarao, M. R. Hill, C. J. Doonan, and C. J. Sumby, *J. Am. Chem. Soc.*, 2013, **135**, 10441-10448.
91. T. Li, J. E. Sullivan, and N. L. Rosi, *J. Am. Chem. Soc.*, 2013, **135**, 9984-9987.
92. C. F. Leong, T. B. Faust, P. Turner, P. M. Usov, C. J. Kepert, R. Babarao, A. W. Thornton, and D. M. D'Alessandro, *Dalton Trans.*, 2013, **42**, 9831-9839.
93. J. Y. Jung, F. Karadas, S. Zulfiqar, E. Deniz, S. Aparicio, M. Atilhan, C. T. Yavuz, and S. M. Han, *Phys. Chem. Chem. Phys.*, 2013, **15**, 14319-14327.
94. P. D. Jadhav, R. V. Chatti, R. B. Biniwale, N. K. Labhsetwar, S. Devotta, and S. S. Rayalu, *Energy & Fuels*, 2007, **21**, 3555-3559.
95. T. Otowa, Y. Nojima, and T. Miyazaki, *Carbon*, 1997, **35**, 1315-1319.
96. A. D. Khawaji, I. K. Kutubkhanah, and J.-M. Wie, *Desalination*, 2008, **221**, 47-69.
97. M. A. Shannon, P. W. Bohn, M. Elimelech, J. G. Georgiadis, B. J. Marinas, and A. M. Mayes, *Nature*, 2008, **452**, 301-310.
98. Z. Hu, Y. Chen, and J. Jiang, *J. Chem. Phys.*, 2011, **134**, 134705.
99. K. S. Park, Z. Ni, A. P. Cote, J. Y. Choi, R. D. Huang, F. J. Uribe-Romo, H. K. Chae, M. O'Keeffe, and O. M. Yaghi, *Proc. Natl. Acad. Sci. USA*, 2006, **103**, 10186-10191.
100. J. C. Tan, T. D. Bennett, and A. K. Cheetham, *Proc. Natl. Acad. Sci. USA*, 2010, **107**, 9938-9943.
101. Z. Hu, L. Zhang, and J. Jiang, *J. Chem. Phys.*, 2012, **136**, 244703.
102. A. A. Adeyemo, I. O. Adeoye, and O. S. Bello, *Toxicol. Environ. Chem.*, 2012, **94**, 1846-1863.
103. E. Haque, J. E. Lee, I. T. Jang, Y. K. Hwang, J. S. Chang, J. Jegal, and S. H. Jhung, *J Hazard Mater*, 2010.
104. C. Chen, M. Zhang, Q. Guan, and W. Li, *Chem. Eng. J.*, 2012, **183**, 60-67.
105. E. Haque, J. W. Jun, and S. H. Jhung, *J Hazard Mater*, 2011, **185**, 507-511.
106. S.H. Huo and X.-P. Yan, *J. Mater. Chem.*, 2012, **22**, 7449.
107. C. Yang, U. Kaipa, Q. Z. Mather, X. Wang, V. Nesterov, A. F. Venero, and M. A. Omary, *J. Am. Chem. Soc.*, 2011, **133**, 18094-18097.
108. Z. Hasan, J. Jeon, and S. H. Jhung, *J Hazard Mater*, 2012, **209-210**, 151-157.
109. N. A. Khan, J. W. Jun, J. H. Jeong, and S. H. Jhung, *Chem. Commun.*, 2011, **47**, 1306-1308.
110. L. Hamon, C. Serre, T. Devic, T. Loiseau, F. Millange, G. Ferey, and G. De Weireld, *J. Am. Chem. Soc.*, 2009, **131**, 8775-8777.
111. F. Ke, L. G. Qiu, Y. P. Yuan, F. M. Peng, X. Jiang, A. J. Xie, Y. H. Shen, and J. F. Zhu, *J Hazard Mater*, 2011, **196**, 36-43.
112. E. Y. Park, Z. Hasan, N. A. Khan, and S. H. Jhung, *J Nanosci Nanotechnol*, 2013, **13**, 2789-2794.
113. T. D. Bennett, P. J. Saines, D. A. Keen, J.-C. Tan, and A. K. Cheetham, *Chem. Eur. J.*, 2013, **19**, 7049-7055.
114. D. F. Sava, M. A. Rodriguez, K. W. Chapman, P. J. Chupas, J. A. Greathouse, P. S. Crozier, and T. M. Nenoff, *J. Am. Chem. Soc.*, 2011, **133**, 12398-12401.
115. W. Xia, X. Zhang, L. Xu, Y. Wang, J. Lin, and R. Zou, *RSC Advances*, 2013, **3**, 11007.
116. H. Jiang, T. Wang, L. Wang, C. Sun, T. Jiang, G. Cheng, and S. Wang, *Microporous Mesoporous Mat.*, 2012, **153**, 124-130.
117. D. Cunha, C. Gaudin, I. Colinet, P. Horcajada, G. Maurin, and C. Serre, *J. Mater. Chem. B*, 2013, **1**, 1101-1108.
118. S. Devautour-Vinot, C. Martineau, S. Diaby, M. Ben-Yahia, S. Miller, C. Serre, P. Horcajada, D. Cunha, F. Taulelle, and G. Maurin, *J. Phys. Chem. C*, 2013, **117**, 11694-11704.
119. D. Cunha, M. Ben Yahia, S. Hall, S. R. Miller, H. Chevreau, E. Elkaïm, G. Maurin, P. Horcajada, and C. Serre, *Chem. Mater.*, 2013, **25**, 2767-2776.
120. M. O. Rodrigues, M. V. de Paula, K. A. Wanderley, I. B. Vasconcelos, S. Alves, Jr., and T. A. Soares, *Int. J. Quantum Chem.*, 2012, **112**, 3346-3355.
121. Y. Chen, V. Lykourinou, C. Vetromile, H. Tran, L.-J. Ming, R. W. Larsen, and S. Ma, *J. Am. Chem. Soc.*, 2012, **134**, 13188-13191.
122. B. Lou and F. He, *New J. Chem.*, 2013, **37**, 309-316.
123. N. J. Hinks, A. C. McKinlay, B. Xiao, P. S. Wheatley, and R. E. Morris, *Microporous Mesoporous Mat.*, 2010, **129**, 330-334.
124. P. S. Wheatley, A. R. Butler, M. S. Crane, S. Fox, B. Xiao, A. G. Rossi, I. L. Megson, and R. E. Morris, *J. Am. Chem. Soc.*, 2006, **128**, 502-509.
125. A. C. McKinlay, B. Xiao, D. S. Wragg, P. S. Wheatley, I. L. Megson, and R. E. Morris, *J. Am. Chem. Soc.*, 2008, **130**, 10440-10444.
126. M. Ma, H. Noei, B. Mienert, J. Niesel, E. Bill, M. Muhler, R. A. Fischer, Y. Wang, U. Schatzschneider, and N. Metzler-Nolte, *Chem. Eur. J.*, 2013, **19**, 6785-6790.

127. P. K. Allan, P. S. Wheatley, D. Aldous, M. I. Mohideen, C. Tang, J. A. Hriljac, I. L. Megson, K. W. Chapman, G. De Weireld, S. Vaesen, and R. E. Morris, *Dalton Trans.*, 2012, **41**, 4060-4066.
128. J. Della Rocca and W. B. Lin, *Eur. J. Inorg. Chem.*, 2010, 3725-3734.
129. K. M. L. Taylor, A. Jin, and W. Lin, *Angew. Chem. Int. Ed.*, 2008, **47**, 7722-7725.
130. N. Lee, S. H. Choi, and T. Hyeon, *Adv. Mater.*, 2013, **25**, 2641-2660.
131. K. E. deKrafft, Z. Xie, G. Cao, S. Tran, L. Ma, O. Z. Zhou, and W. Lin, *Angew. Chem. Int. Ed.*, 2009, **48**, 9901-9904.
132. L. Chen, H. Zheng, X. Zhu, Z. Lin, L. Guo, B. Qiu, G. Chen, and Z.-N. Chen, *Analyst*, 2013, **138**, 3490-3493.
133. T. Baati, L. Njim, F. Neffati, A. Kerkeni, M. Bouttemi, R. Gref, M. F. Najjar, A. Zakhama, P. Couvreur, C. Serre, and P. Horcajada, *Chemical Science*, 2013, **4**, 1597.
134. E. A. Fluegel, A. Ranft, F. Haase, and B. V. Lotsch, *J. Mater. Chem.*, 2012, **22**, 10119-10133.